

# Preparation of Nanostructured Iron Oxide Particles and Their Surface Functionalization with Oleic Acid, 3-aminopropyltrimethoxysilane and Silver Nanoparticles

(Submitted: June 20, 2019; Accepted: December 15, 2019)

Nur Uddin Ahamad<sup>1\*</sup>, Nur-E-Jannat<sup>2</sup>, Abdul Halim<sup>3</sup>, Muhammad Raek Zaman<sup>4</sup>,  
Abu Bin Hasan Susan<sup>5</sup>, Md. Mohibul Alam<sup>6</sup>

<sup>1,2,3,4</sup> Department of Chemistry, Shahjalal University of Science and Technology, Sylhet-3114

<sup>5</sup> Department of Chemistry, Dhaka University

<sup>6</sup> Department of CEP, Shahjalal University of Science and Technology, Sylhet-3114

\*Corresponding author: nur-che@sust.edu

## Abstract

In this article, preparation of magnetic nanostructured iron oxide particles (IOs) and their surface functionalization with oleic acid, 3-Aminopropyltrimethoxysilane (APTMS) and Ag nanoparticles are reported. IOs were prepared by co-precipitation method and colloidal silver nanoparticles were synthesized by polyol method. The nanoscale IOs (<100nm) exhibited paramagnetic property and surface functionalization did not alter its magnetism. Colloidal stability of IOs particles is dependent on the nature of the surfactants. Necked IOs, and IOs functionalized with APTMS and Ag nanoparticles are polydisperse in size while IOs functionalized with oleic acid are monodisperse. Such functionalized IOs can be employed in medical diagnostics, environmental remediation and energy harvesting technology.

**Keywords:** Co-precipitation; polyol method; Iron Oxide particles; silver nanoparticles; APTMS; oleic acid.

## 1. Introduction

Nanoparticles in the nanometer-size range have recently attracted the attention of researchers because of their unique physical and chemical properties [1]. Nano-sized materials, as compared to their bulk counterparts, exhibit new characteristic optical, electrical and magnetic properties due to the enhanced surface to volume ratio and quantum confinement effects emerging in these size ranges [2,3,4]. These new features of nanoparticles offer them the possibility to be used in a wide range of technological (magnetic data storage, sensor, refrigeration), environmental (catalysts, adsorbent, hydrogen storage), energy (lithium-ion batteries, solar cells) and biomedical applications [5].

Nanostructured Metal oxides possess unique properties that include wide bandgaps [6], high dielectric constants [7], reactive electronic transitions [8] and good electrical [9], optical [10] and electrochromic characteristics [11] as well as superconductivity [12]. Therefore, metal-oxides are some of the most fascinating functional materials and have been widely exploited in various technological applications.

Magnetic NPs are of great interest for researchers from a broad range of disciplines, including catalysis, magnetic fluids, data storage, and bioapplications, due to their unique magnetic properties such as superparamagnetism, high coercivity, low Curie temperature, high magnetic susceptibility, etc [13].

Iron oxide (IO) have received special attention because of their variety of scientific and technological applications such as catalysis [14] [16], adsorbent [15], antimicrobial activity, magnetic storage media, magnetic refrigeration, magnetic resonance imaging (MRI) [17, 18], hyperthermic cancer treatments, cell sorting and targeted drug delivery [19]. Besides, it has also been widely used in biomedical research because of its biocompatibility and magnetic properties [19]. Plasmonic silver nanoparticles when integrated on magnetic iron oxide surface resulting a multifunctional magnetoplasmonic nanocomposite which produce electron/hole pairs upon excitation of plasmonic nanoparticles by induced electric field [20].

However, it is a technological challenge to control size, shape, stability, and dispersibility of NPs in desired solvents. Magnetic iron oxide NPs have a large surface-to volume ratio and therefore possess high surface energies [21]. Consequently, they tend to aggregate to minimize the surface energies. Moreover, the naked iron oxide NPs have high chemical activity, and are easily oxidized in air (especially magnetite), generally resulting in loss of magnetism and dispersibility. Therefore, providing proper surface coating and developing some effective protection strategies to keep the stability of magnetic iron oxide NPs is very important. These strategies comprise grafting of or coating with organic molecules, including small organic molecules or surfactants, polymers, and biomolecules, or coating with an inorganic layer,

such as silica, metal or nonmetal elementary substance, metal oxide or metal sulfide. Practically, it is worthy that in many cases the protecting shells not only stabilize the magnetic iron oxide NPs, but can also be used for further functionalization for many applications.

In this research work, we intended to functionalize iron oxide with oleic acid, amino-propyl-tri-methyl-silane (APTMS) and with plasmonic metal silver (Ag) nanoparticles to prepare functional nanomaterials that find application in photocatalysis, photovoltaics and environmental remediation.

## 2. Experimental

### 2.1. Materials

Ferrous sulfate (Merck), Ferric chloride (Merck), Ammonia (25%, Merck), Distilled water, Ethylene glycol (Sigma-Aldrich), Silver nitrate (Merck), Polyvinylpyrrolidone (PVP, Mw 55000, Merck), 3-Aminopropyltrimethoxysilane (APMTS, Sigma-Aldrich), Methanol (Merck), Ethanol (95%, Merck). All chemicals were used without further purification.

### 2.2. Methods

#### 2.2.1. Preparation of IOs

Iron oxide nanoparticles were synthesized by the reverse co-precipitation method where iron(II) chloride and iron(III) chloride were used as the iron precursors and ammonium hydroxide was used as the base as reported earlier [22]. Briefly, a mixed solution of  $\text{FeCl}_2 \cdot 4\text{H}_2\text{O}$  and  $\text{FeCl}_3 \cdot 6\text{H}_2\text{O}$  was added to an ammonium hydroxide solution to get the precipitate. Formation of IOs was characterized by its characteristic FTIR spectrum, response to external magnetic field and SEM-EDS.

#### 2.2.2. Preparation of Colloidal Ag Nanoparticles

A colloidal solution of silver nanoparticles is synthesized by a modified polyol process developed by Xia et al [23,24]. In a typical synthesis, 10 mL of EG is placed in a 100-mL triple-necked round-bottom flask and heated at 140 °C for 1 h under stirring with Teflon-coated magnetic stirring bar using a temperature-controlled heating mantle. While EG is heated, EG solutions containing  $\text{AgNO}_3$  and PVP are prepared. 6 ml of both  $\text{AgNO}_3$  and PVP solutions are added dropwise simultaneously in the hot reaction mixture using pipettes. The resulting solution was heated for 1 h. The final product is cooled to room temperature and centrifuged by ethanol. The plasmonic signature and the morphology of the Ag were characterized by UV-Visible and SEM-EDS respectively.

#### 2.2.3. Functionalization of IOs with Ag Nanoparticles

Ag functionalized IOs are fabricated by silanisation

process as reported elsewhere [25]. Briefly, 1% APTMS solution is prepared in ethanol. 5 mg of IOs is added in 10 ml APTMS solution. Then 2 ml of as prepared Ag nanoparticles solution is added in the beaker. The solutions mixture is kept for 1 hr. After 1 hr., the IOs-Ag materials were washed for 5 mins with ethanol. Washing cycle is repeated 15 times. Then the materials are filtered with filter paper and dried at room temperatures. The FTIR spectra of bare-IOs and Ag/IOs are recorded respectively.

#### 2.2.4. Functionalization of IOs with Oleic Acid

10 ml aqueous solution of IOs (1mg/ml) was mixed with  $5 \times 10^{-4}$  M oleic acid solution in methanol and stirred for 6 hours till all the nanoparticles get precipitated at the bottom. After decanting water-methanol solution, addition of 10 ml toluene and 15 minutes' sonication in the precipitate resulted in clearly dispersed functionalized NPs in toluene [26].

#### 2.2.5. Surface Functionalization of Synthesized $\text{Fe}_3\text{O}_4$ Nanoparticles with APTMS

1% APTMS solution was prepared in methanol from which 10 ml solution was taken in a beaker. 5.0 mg of IOs was added in the beaker containing 10 ml of 1% APTMS. The solution-mixture was stirred for 1h. After 1h of stirring, the solution mixture was centrifuged and precipitate was collected. The precipitate was washed 15 times with ethanol by centrifuge and finally the wet precipitate was filtered and dried at room temperature [25].

## 3. Result and Discussion

### 3.1. Magnetic Properties of IOs

When placed an external magnetic bar in the vicinity of the container containing the as synthesized IOs, they are attracted by the magnetic bar and formed spikes, as shown in Figure 1, which revealed the magnetic behaviour of IOs. The spike like structures indicate the formation of  $\text{Fe}_3\text{O}_4$  [27].



Figure 1: Response to external magnetic field of the as synthesized IOs

### 3.2. Optical Absorption and Emission Properties of Ag Nanoparticles

It is known that colloidal silver nanoparticles exhibit yellowish color (Figure 2.a, inset) in solution due to excitation of surface plasmon in the visible region of spectrum. Formation of silver nanoparticles was confirmed by its characteristic surface plasmon resonance absorption peaks in its UV-Vis spectrum (Figure 2). The absorption spectrum of silver nanoparticles consisted of multiple resonance peaks centering at 360 nm, 410 nm and 450 nm (Fig.2a), which revealed the formation of anisotropic silver nanoparticles [28].

Colloidal Ag nanoparticles also exhibited photoluminescence property at room temperature. Emission spectrum of colloidal Ag nanoparticles is shown in Figure 2.b. The visible luminescence of silver is due to the excitation of electrons from occupied d bands into states above the Fermi level and then, electron-phonon and hole-phonon scattering process take place results in energy loss and subsequently, radiative recombination of an electron from an occupied sp band with the hole takes place. Emission spectrum of colloidal Ag nanoparticles is shown in Figure 2.b. Excitation of the sample with 370 nm wavelength produced emission spectrum with maximum intensity at 453 nm showed photoluminescence property in the visible region[29].

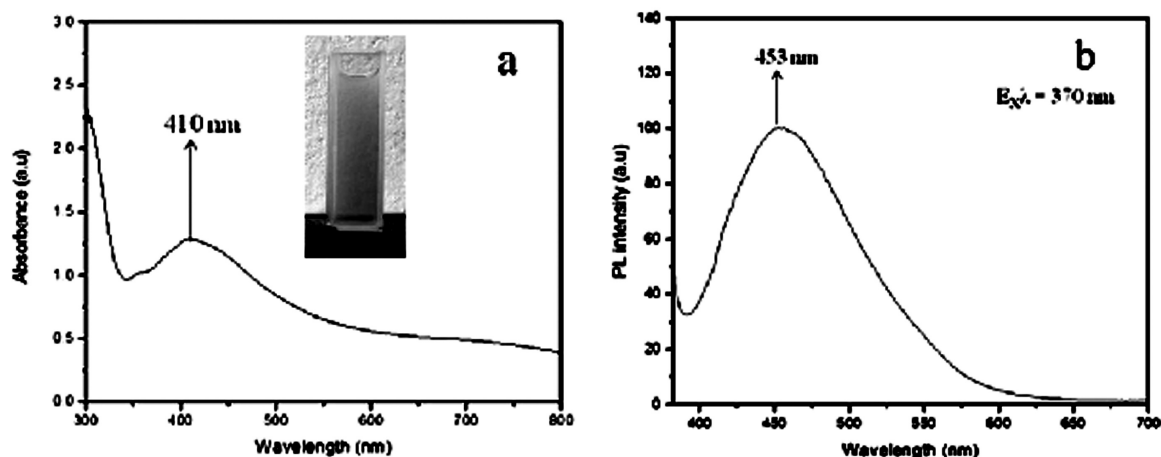


Figure 2: (a) UV-Visible absorption and (b) emission spectra of colloidal Ag nanoparticles (in set picture, a)

### 3.3. Fourier Transform Infrared (FTIR) Spectral Analysis

#### 3.3.1. FTIR spectrum of the IOs

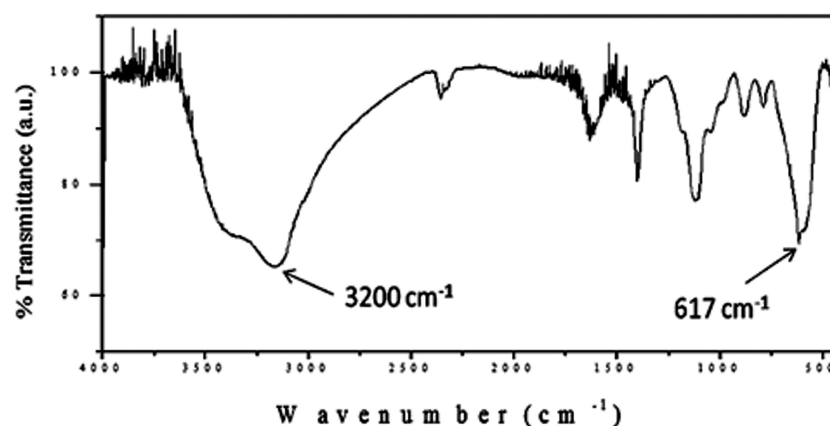


Fig.3. FTIR spectrum of IOs.

The characteristic FTIR peaks are shown in Figure 3. The peak at  $3200\text{cm}^{-1}$  is attributed to the stretching vibrations of -OH, the range of frequency of the -OH group is  $3650\text{--}3200\text{ cm}^{-1}$ , which is assigned to -OH absorbed by IOs and the peak centering at  $617\text{ cm}^{-1}$  is attributed to the Fe-O bond vibration of  $\text{Fe}_3\text{O}_4$ [30].

#### 3.3.2. FTIR Spectrum of IOs Functionalized with Oleic Acid

To confirm the functionalization of IOs with Oleic acid, FTIR spectrum of pure oleic acid was recorded which is shown in Figure 4.

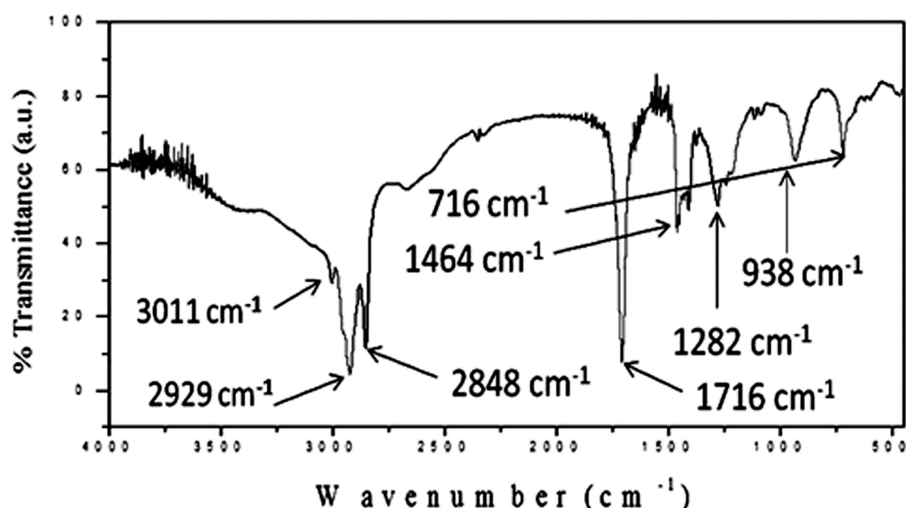


Fig. 4: The FTIR spectrum of oleic acid(OA)

Two sharp peaks at 2929, 2848  $\text{cm}^{-1}$  were attributed to the asymmetric  $\text{CH}_2$  stretch and the symmetric stretch, respectively. The intense peak at 1716  $\text{cm}^{-1}$  was derived from the  $\text{C}=\text{O}$  stretch, and the peak at 1282  $\text{cm}^{-1}$

reflected the presence of  $\text{C}-\text{O}$  stretch. The  $\text{O}-\text{H}$  in plane and out of plane bands appeared at 1464 and 938  $\text{cm}^{-1}$  respectively which is consistent with literature[30]. The characteristic peaks of IOs functionalized with oleic acid is shown in Figure 5.

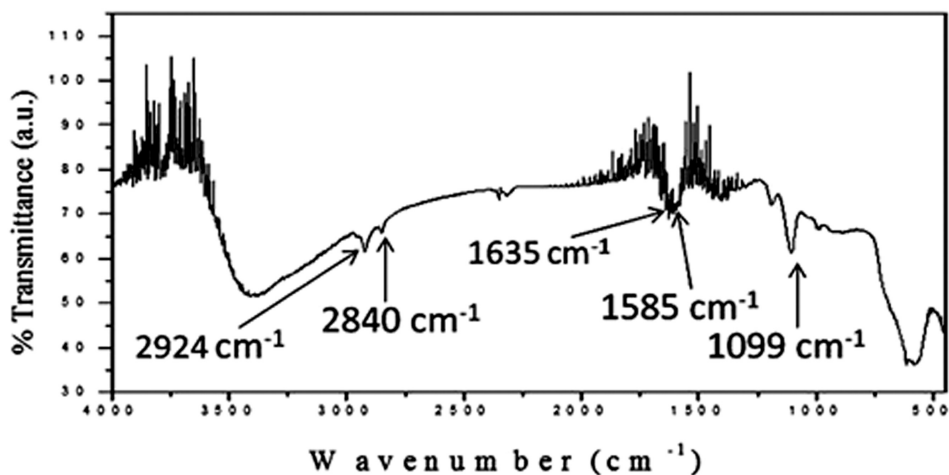


Fig. 5. The FTIR spectrum of IOs functionalized with oleic acid

The asymmetric  $\text{CH}_2$  stretch and symmetric  $\text{CH}_2$  stretch of oleic acid shifted to 2924 and 2840  $\text{cm}^{-1}$  respectively. The shifting of these peaks to a lower frequency region indicate that the hydrocarbon chains in the monolayer surrounding the nanoparticles were in a closed packed crystalline state. It is noticed that  $\text{C}=\text{O}$  stretching band of the carbonyl group appears at 1716  $\text{cm}^{-1}$  in pure oleic acid, Figure 4, which is absent in the spectrum, Figure 5, of the functionalized IOs. In addition, two new bands appeared at 1585 and 1635  $\text{cm}^{-1}$ , which were characteristic of the asymmetric  $\nu_{\text{as}}(\text{COO}^-)$  and  $\nu_{\text{ns}}(\text{COO}^-)$  stretch. This result indicates that the bonding pattern of the carboxylic acids on the surface of the nanoparticles

was a combination of molecules bonded symmetrically and molecules bonded at an angle to the surface. A strong adsorption at 1099  $\text{cm}^{-1}$  arose from  $\text{C}-\text{O}$  single bond stretching. These results revealed that oleic acid molecules were chemisorbed onto the IOs as a carboxylate[30].

### 3.3.3. FTIR Spectrum of IOs Functionalized with APTMS

To confirm the functionalization of IOs with APTMS, FTIR spectrum of pure APTMS was recorded as a reference which is shown in Figure 6.

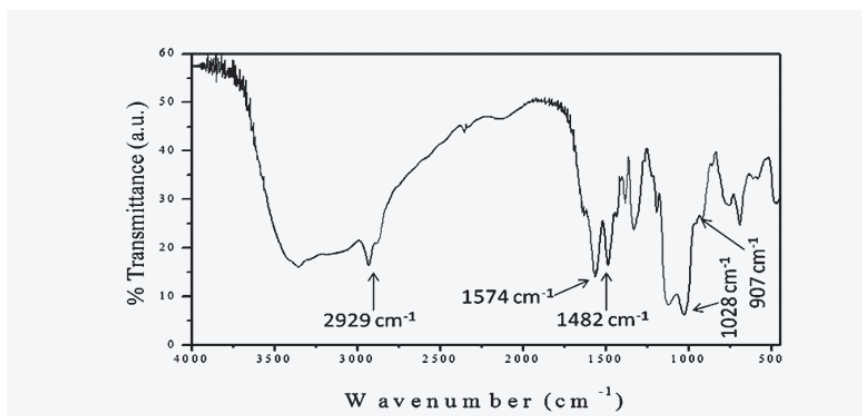


Fig. 6. The Infrared spectrum of APTMS

FTIR spectrum of APTMS clearly shows a sharp band at 2929  $\text{cm}^{-1}$  which is attributed to the C-H stretch. The two intense peaks at 1574 and 1482  $\text{cm}^{-1}$  were derived from the  $\text{NH}_2$  and methylene groups respectively. The Si-O-Si

bridge and Si-O bonds appeared at 1028  $\text{cm}^{-1}$  and 907  $\text{cm}^{-1}$  respectively[31].

Figure 7 shows the FTIR spectrum of IOs functionalized with APTMS.

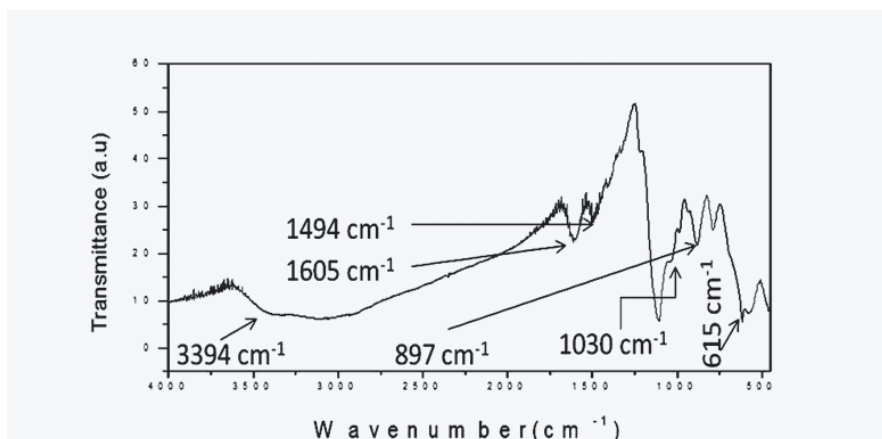


Fig. 7. The Infrared spectrum of IOs functionalized with APTMS

In this spectrum, peak around 1605  $\text{cm}^{-1}$  is assigned to the  $-\text{NH}_2$  terminal of APTMS. The  $\text{CH}_2$  bending was found at 1494  $\text{cm}^{-1}$ , the Si-O-Si bridges were appeared at 1030  $\text{cm}^{-1}$ , and the Si-O bond at 915  $\text{cm}^{-1}$ . The peak at 3394  $\text{cm}^{-1}$  is attributed to the stretching vibrations of  $-\text{OH}$  which is assigned to  $-\text{OH}$  absorbed by IOs and the peak at 615  $\text{cm}^{-1}$  is attributed to Fe-O bond vibration of IOs[30, 31]. Due to the functionalization of IOs using a

chemical linker APTMS Fe-O bond becomes weaker. In this bond, bond length of Fe-O is increased. So, the band shifts to the lower wavenumber i.e.; longer wavelength.

### 3.3.4. FTIR Spectrum of Nanocomposite Consisted of IOs and Ag Nanoparticles

The characteristic peaks in the FTIR spectrum of the nanocomposite consisted to IOs.APTMS.Ag is shown in Figure 8.

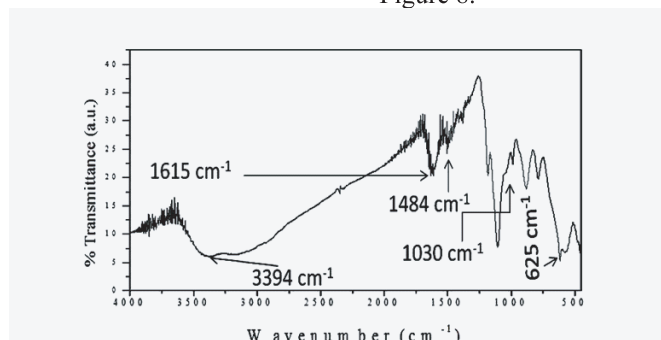


Fig. 8. The Infrared spectrum of nanocomposite IOs.APTMS.Ag

The peak around  $1615\text{ cm}^{-1}$  is ascribed to the  $-\text{NH}_2$  terminal of APTMS. The  $-\text{CH}_2$  bending was found at  $1484\text{ cm}^{-1}$ . The peak at  $3394\text{ cm}^{-1}$  is attributed to the stretching vibrations of  $-\text{OH}$ , which is assigned to  $-\text{OH}$  absorbed by IOs. The peak at  $625\text{ cm}^{-1}$  is attributed to the Fe-O bond vibration in nanocomposite [30, 31, 32]. It is hypothesized that due to electron tunneling from Ag nanoparticles (plasmonic particles) to conduction band of IOs, electron density in Fe-O bond is increased.

Because of increased electron density, the bond strength is increased and therefore wavenumber of absorbed radiation is increased compared to that of in Fe-O bond in necked IOs.

### 3.4. Morphologies of the Nanostructures

To obtain detailed information about the morphology and the particle size of the nanostructures, scanning electron microscopy (SEM) was employed.

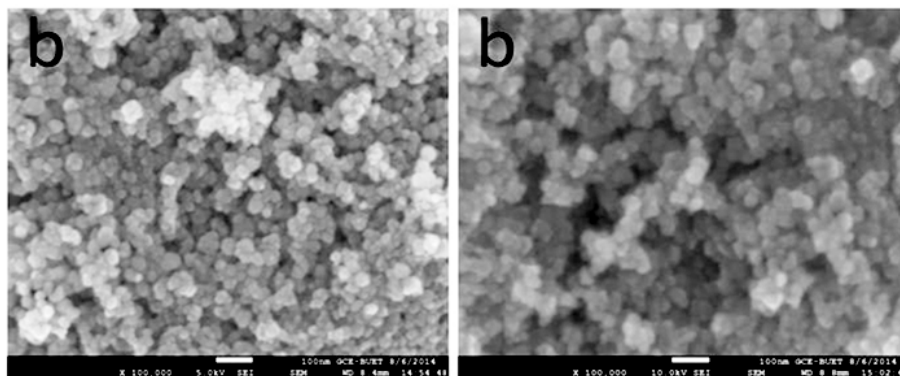


Fig. 9(b). The SEM images of  $\text{Fe}_3\text{O}_4$  functionalized with oleic acid.

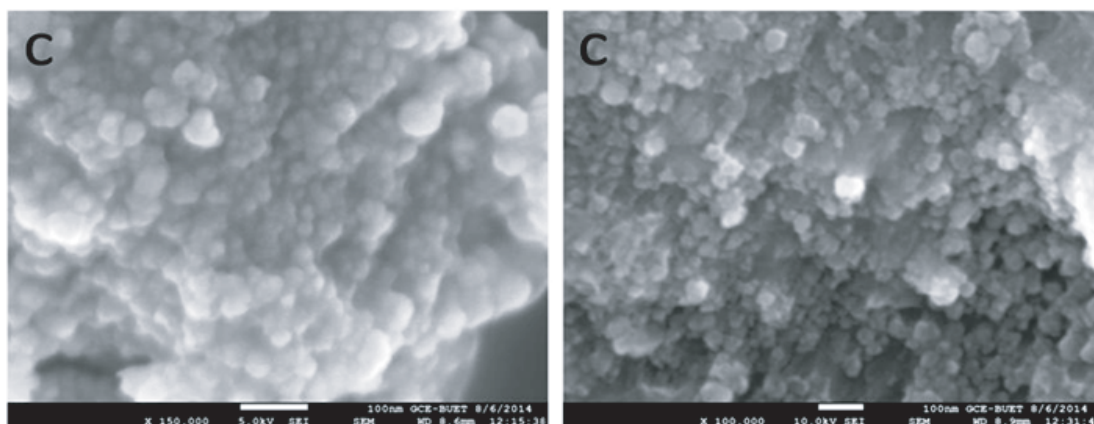


Fig. 9(c). The SEM images of  $\text{Fe}_3\text{O}_4$  functionalized with APTMS

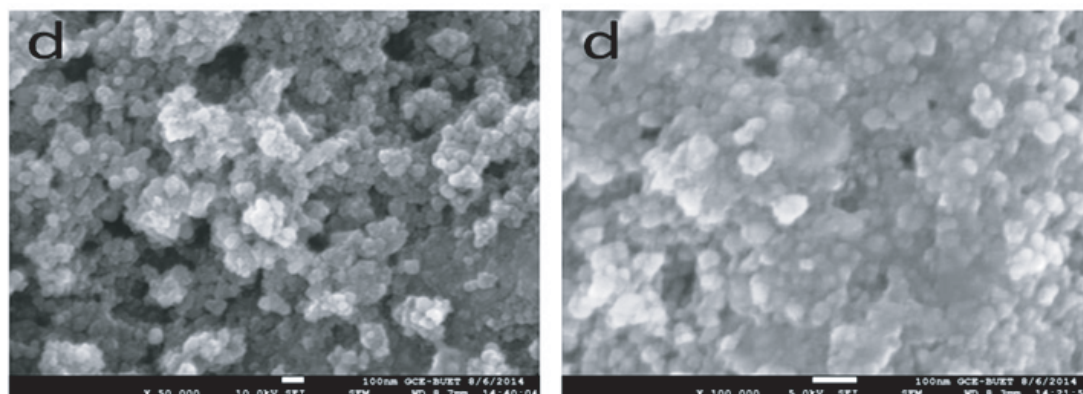


Fig. 9(d). The SEM images of the nanocomposite consisted of  $\text{Fe}_3\text{O}_4$ , APTMS and Ag nanoparticles.

Figure9 shows the SEM images of pure IOs and its functionalized counterparts. It is evident from the images (from scale bar) that all four types of nanostructures had their dimensions in nanoscale range i.e.; diameter below 100 nm. The nanostructures were quasi-spherical in shape. However, except oleic acid functionalized IOs, which was monodispersed in size and formed stable colloids, the other three types of nanostructures were polydispersed in size and formed less stable colloids. This is because of formation of aggregates either in the

absence of any surfactant (pure IOs) or presence of APTMS molecules which form crossed-linked polymer. However, Fe<sub>3</sub>O<sub>4</sub> functionalized with oleic acid gives monodispersed and stable colloidal IOs.

**3.5. Energy Dispersive X-Ray Spectroscopic (EDS) Analysis**

Energy dispersive X-ray spectroscopic (EDS) analysis of the samples was carried out to get information on elemental compositions of the nanostructured samples.

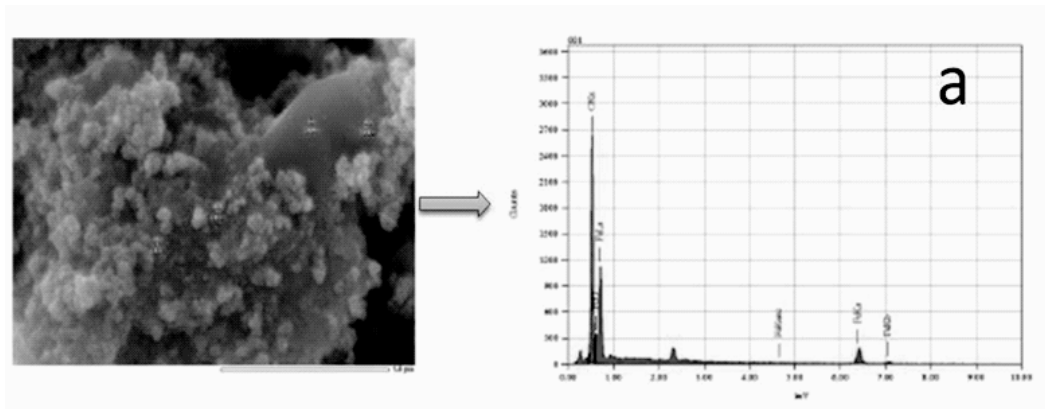


Fig. 10(a). The EDS spectrum of IOs particles

The composition components of IOs is given in the following table.

Element	keV	Mass %	Sign a	Atom %
<b>OK</b>	<b>0.525</b>	<b>40.41</b>	<b>0.28</b>	<b>70.30</b>
<b>Fe K</b>	<b>6.398</b>	<b>59.59</b>	<b>1.49</b>	<b>29.70</b>
<b>Total</b>		<b>100.00</b>		<b>100.00</b>

Table3(a): The composition of IOs nanostructures

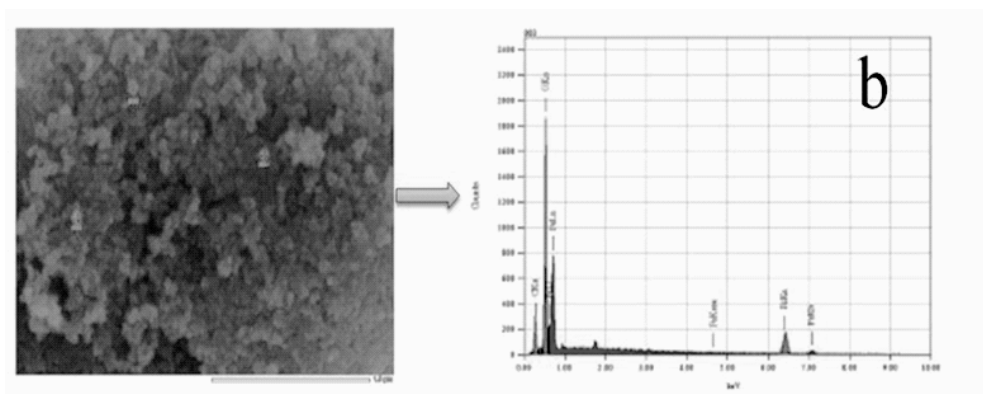
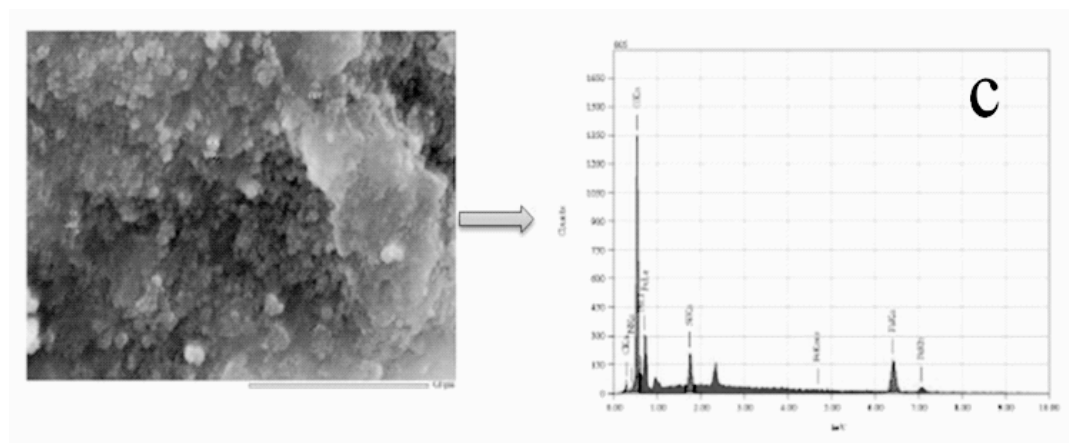


Fig. 10(b). The EDS spectrum of IOs functionalized with oleic acid

Element	keV	Mass %	Signa	Atom %
C K	0.277	10.86	0.14	22.75
O K	0.525	33.05	0.28	51.97
Fe K	6.398	56.09	1.45	25.27
<b>Total</b>		<b>100.00</b>		<b>100.00</b>

Table 3(b). The composition of oleic acid functionalized IOs.



10(c). The EDS spectrum of IOs functionalized with APTMS

Element	keV	Mass %	Signa	Atom %
C K	0.277	2.45	0.02	6.51
N K	0.392	0.17	0.04	0.38
O K	0.525	25.23	0.09	50.27
Si K	1.739	2.92	0.08	3.31
Fe K	6.398	69.24	0.76	39.53
<b>Total</b>		<b>100.00</b>		<b>100.00</b>

Table 3(c): The composition of IOs functionalized with APTMS



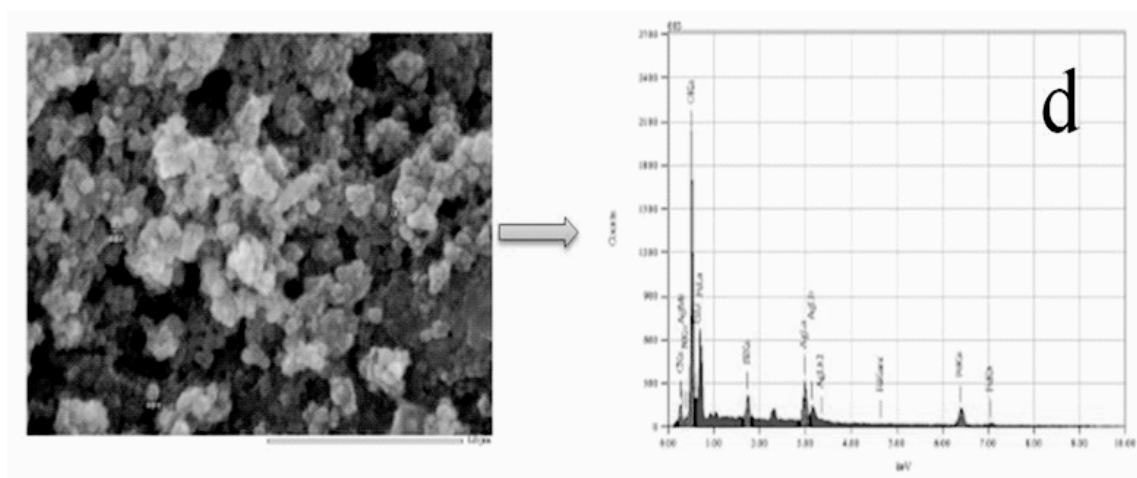


Fig. 10(d). EDS spectrum of nanocomposite consisted of IOs-APTMS-Ag nanoparticles.

Element	keV	Mass %	Sign a	Atom %
C K	0.277	3.60	0.02	8.06
N K	0.392	0.45	0.06	0.87
O K	0.525	39.81	0.13	66.97
Si K	1.739	1.98	0.06	1.89
Fe K	6.3983	37.39	0.54	18.02
Ag L	2.983	16.77	0.24	4.18
<b>Total</b>		<b>100.00</b>		<b>100.00</b>

Table. 3(d). The composition component of nanocomposite consisted of IOs-APTMS-Ag nanoparticles.

Point and shoot analysis were employed to determine the presence and distribution of elements in the samples. The major components of the spot of the samples in the EDS spectra (the resolution of the spectra are poor as the original file received were image files and could not be reproduced), are shown in Figure 10. The elemental analysis of the samples corroborated with the desired materials and consisted with FTIR results of the corresponding samples.

#### 4. Conclusion

In this research, preparation of magnetic nanostructured iron oxide particles and their surface functionalization with oleic acid, APTMS and Ag nanoparticles were accomplished. Surface functionalization of IOs did not change its magnetic property. However, colloidal property of IOs particles is dependent on the nature of the surfactants.

The particle size of IOs and IOs functionalized with APTMS and Ag nanoparticles are polydisperse while IOs functionalized with oleic acid are monodisperse. Research is ongoing to unveil the phase of the as synthesized IOs particles i.e.; Fe<sub>3</sub>O<sub>4</sub> or Fe<sub>2</sub>O<sub>3</sub>. Such functionalized nanoparticles (IOs-OA, IOs-APTMS) and nanocomposite (IOs-APTMS-Ag nanoparticles) can be employed in biomedical application, environmental remediation and energy harvesting technology.

#### 5. Acknowledgement

Financial assistance was provided by MOST project-2015-16/Phy's 41. We are thankful to Professor Syed Shamsul Alam, Department of Chemistry, SUST and Dr. Abu Ali Ibn Sina, Department of BMB, SUST for providing APTMS and AgNO<sub>3</sub> respectively.

## 6. References

- Koutzarova, T., Kolev, S., Ghelev, C., Paneva, D., Nedkov, I., Microstructural Study and Size Control of Iron Oxide Nanoparticles Produced by Microemulsion Technique, *Phys. Stat. Sol.* 2006, C 3, 1302 - 1307.
- Pikethly, M. J., *Nanomaterials- The Driving Force, Materials Today* 2004, 7, 20.
- Moumen, M., Bonville, P. and Pileni, M.P., Control of the Size of Cobalt Ferrite Magnetic Fluids: Mössbauer Spectroscopy, *J. Phys. Chem.* 1996, 100, 14410.
- Li, L., Deng, Y., Song, X., Jin, Z., and Zhang, Y., Fabrication of Double-Doped Magnetic Silica Nanospheres and Deposition of Thin Gold, *Bull. Korean Chem. Soc.* 2003, 24, 957.
- Umut, E., Surface Modification of Nanoparticles Used in Biomedical Applications, Chapter- 8, *Modern Surface Engineering Treatments*, page 185-208.
- Emeline, A. V., Kataeva, G.V., Panasuk, A.V., Ryabchuk, V.K., Sheremetyeva, N.V., Serpone, N., Effect of Surface Photoreactions on the Photocoloration of a Wide Band Gap Metal Oxide: Probing Whether Surface Reactions Are Photocatalytic, *J. Phys. Chem. B* 2005, 109, 5175-5185.
- Gutowski, M., Jaffe, J. E., Liu, C. L., Stoker, M., Hegde, R. I., Rai, R. S., Tobin, P. J., Thermodynamic Stability of High-K Dielectric Metal Oxides and in Contact with Si and SiO<sub>2</sub>, *Appl. Phys. Lett.* 2002, 80, 1897-1899.
- Chen, K., Bell, A. T., Iglesia, E., The Relationship between the Electronic and Redox Properties of Dispersed Metal Oxides and Their Turnover Rates in Oxidative Dehydrogenation Reactions, *J. Catal.* 2002, 209, 35 - 42.
- Mavrou, G., Galata, S., Tsipas, P., Sotiropoulos, A., Panayiotatos, Y., Dimoulas, Evangelou, A., E. K., Seo, J. W., Dieker, C., Very high- $\kappa$  ZrO<sub>2</sub> with La<sub>2</sub>O<sub>3</sub> (LaGeOx) Passivating Interfacial Layers on Germanium Substrates, *J. Appl. Phys.* 2008, 93, 212904(1-3).
- Zhu, Y., Zong, R., Zhu, Y., Liu, Y., Zhang, M., Lv, Y., Liu, D., Defect-Related Photoluminescence and Photocatalytic Properties of Porous ZnO Nanosheets, *J. Mater. Chem. A*, 2014, 2, 15377-15388.
- Rosseinsky, D. R., Mortimer, R. J., *Electrochromic Systems and the Prospects for Devices*, *Adv. Mater.* 2001, 13, 783 - 793.
- Yang, H. D., Lin, C. P., Sun, Y. C. Kang, C. L. Huang, K. Takada, Sasaki, T., Sakurai, H., and Muromachi, E. T., Evidence of Nodal Superconductivity in Na<sub>0.35</sub>CoO<sub>2</sub> · 1.3 H<sub>2</sub>O: A Specific-Heat Study, *Physical Review B* 71. 2005, 020504, 020504(1-4).
- Wu, W., He, Q., and Jiang, C. Magnetic Iron Oxide Nanoparticles: Synthesis and Surface Functionalization Strategies, *Nanoscale Res Lett.* 2008, 3, 397-415.
- Kormann, C., Bahnemann, D.W. and Hoffmann, M. R., Is Iron Oxide (Hematite) an Active Photocatalyst? A Comparative Study: A-Fe<sub>2</sub>O<sub>3</sub>, ZnO, TiO<sub>2</sub>, *Journal of Photochemistry and Photobiology, A. Chemistry* 1989, 48, 161-169.
- Carlos, L., Einschlag, F. S., González, M. C., and Mártire, D. O., Applications of Magnetite Nanoparticles for Heavy Metal Removal from Wastewater, *Waste Water-Treatment Technologies and Recent Analytical Developments* 2013, 3, 64-73.
- Wu, W., Jiang, C. and Roy, V. A. L., Recent Progress in Magnetic Iron Oxide-Semiconductor Composite Nanomaterials as Promising Photocatalysts, *Nanoscale* 2015, 7, 1-49.
- Mornet, S., Vasseur, S., Grasset, F., Verveka, P., Goglio, G., Demourgues, A., Portier, J., Pollert, E., Duguet, E., Ferromagnetic Microdisks as Carriers for Biomedical Applications *Prog. Solid State Chem.* 2006, 34, 237
- Li, Z., Wei, L., Gao, M. Y., Lei, One-Pot Reaction to Synthesize Biocompatible Magnetite Nanoparticles, *H. Adv. Mater.* 2005, 17, 1001.
- Amstad, E., Textora, M. and Reimhult, E., Nanoscale, Stabilization and Functionalization of Iron Oxide Nanoparticles for Biomedical Applications 2011, 3, 2819
- Banerjee, S., Pillai, S. C., Falaras, P., O'Shea, K. E., Byrne, J. A., and Dionysiou, D. D., New Insights into the Mechanism of Visible Light Photocatalysis, *J. Phys. Chem. Lett.* 2014, 5, 2543-2554
- Wu, W., He, Q., Jiang, C., Magnetic Iron Oxide Nanoparticles: Synthesis and Surface Functionalization Strategies, *Nanoscale Res Lett* 2008, 3, 397-415
- Chan, D. C. F., Kirpotin, D. B., Bunn, P. A., Synthesis and Evaluation of Colloidal Magnetic Iron Oxides for the Site-Specific Radio Frequency Induced Hyperthermia of Cancer, *Journal of Magnetism and Magnetic Materials* 1993, Vol. 122, No. 1, 374-378
- Ahamad, N., Prezgot, D. and Ianoul, A., Patterning Silver Nanocubes in Monolayers Using Phase Separated Lipids as Templates. *J. Nanopart. Res.* 2012, 14, 724.
- Nur, A., Adam, B., Anatoli, I., Optimizing Refractive Index Sensitivity of Supported Silver Nanocubes. *Phys. Chem. C.* 2012, 116, 185-192.
- Ahamad, N., Al Amin, M., Ianoul, A., Distance Dependent Surface Enhanced Raman and Fluorescence by Supported 2D Assembly of Plasmonic Metal Nanoparticles. *Chemistry* 2013, 25, 9226-9232.

26. Bloemen, M., Brullot, W., Luong, T., Geukens, N., Gils, A., Verbiest, T., Improved Functionalization of Oleic Acid-Coated Iron Oxide Nanoparticles for Biomedical Applications, *J Nanopart. Res* 2012, 14, 1100.
27. Lu, A., Salabas, E., Schüth, F., Magnetic Nanoparticles: Synthesis, Protection, Functionalization and Application, *Angew Chem. Int. Ed.* 2007, 46 (8), 1222-1244.
28. Wiley, B., Sun, Y., Mayers, B., Xia, Y., Shape-Controlled Synthesis of Metal Nanostructures: The Case of Silver, *Chem. Eur. J.* 2005, 11, 454 - 463.
29. Benami, A., Lopez-Suarez, A., Fernandez, L., Sosa, A., Wong, J., Esqueda, J., and Oliver, A., Enhancement and Quenching of Photoluminescence from Silicon Quantum Dots by Silver Nanoparticles in a Totally Integrated Configuration, *AIP Advances* 2012, 2, 012193.
30. Yosefine, A., Youngjin, S., Junghwan, O., Controlling the Optimum Dose of AMPTS Functionalized-Magnetite Nanoparticles for Hyperthermia Cancer Therapy, *Appl. Nanosci.* 2011, 1, 237-246.
31. Suddai, A., Nuengmatcha, P., Sricharoen, P., Limchoowong, N., and Chantha, S., Feasibility of Hard Acid-Base Affinity for the Pronounced Adsorption Capacity of Manganese (II) Using Amino-Functionalized Graphene Oxide, *RSC Adv.* 2018, 8, 4162-4171.
32. Guo, H., Zhao, A., Wang, R., Wang, D., Wang, L., Gao, Q., Sun, H., Li, L., H, Q., Generalized Green Synthesis of Fe<sub>3</sub>O<sub>4</sub>/Ag Composites with Excellent SERS Activity and Their Application in Fungicide Detection, *J Nanopart Res*, 2015, 17, 494, 1-10.